Available online at www.sciencedirect.com
SCIENCE DIRECT
Journal of Catalysis 242 (2006) 195–206
JOURNAL OF CATALYSIS
www.elsevier.com/locate/jcat

Isomerization and disproportionation of m-xylene in a zeolite with 9- and 10-membered ring pores: Molecular dynamics and catalytic studies

Francisco J. Llopis [a], German Sastre [b], Avelino Corma [b,*]

[a] *Departamento de Ingeniería Química, Universidad de Valencia, c/Dr. Moliner 50, 46100 Burjassot, Valencia, Spain*
[b] *Instituto de Tecnología Química, UPV-CSIC, Universidad Politécnica de Valencia, Avda. de los Naranjos s/n, 46022 Valencia, Spain*

Received 15 March 2006; revised 10 May 2006; accepted 27 May 2006

Available online 12 July 2006

Abstract

The unique pore topology of zeolite ITQ-13 with 9-membered ring (MR) channels intersected by perpendicular 10-MR channels and larger void space with 10-MR cross-sections was studied for *meta*-xylene isomerization and disproportionation. Product distribution was interpreted on the basis of pore topology and compared with zeolites with 12-MR (β), 10-MR, and intersecting 12-MR cavities (NU-87), as well as 10-MR (ZSM-5) zeolites. The presence of cavities allows more space for bulky intermediates and/or products and also provides room for molecules to drive consecutive reactions toward thermodynamic equilibrium. Channels, on the other hand, allow diffusion without trapping if their free diameters are large enough. The 9-MR channels are not suitable for diffusion of *para*-xylene, *ortho*-xylene, *meta*-xylene, or 1,2,4-trimethylbenzene. Catalytic experiments and atomistic molecular dynamics are used to interpret the behavior of ITQ-13 and explain the results in comparison with other structures.

Keywords: m-Xylene; Isomerization; Zeolite; ITQ-13; Molecular dynamics

1. Introduction

The great success of zeolites as acid catalysts is due to these materials' highly desirable catalytic properties, including strong acidity, controlled site density, high thermal and hydrothermal stability, and shape selectivity toward reactants, products, and transition states [1–4]. Among those properties, shape selectivity effects in catalysis are particularly relevant because they have been responsible for many new industrially important processes [5]. Among those, we highlight here the isomerization of C_8 alkyl aromatics and the disproportionation of toluene to produce *para*-xylene [6–12]. An important step forward in selectivity was achieved when ZSM-5 zeolite was introduced as a catalyst. This zeolite is formed by two intersecting 10-membered ring (MR) channels with 5.1×5.5 Å and 5.3×5.6 Å pore diameters, which are close to the kinetic diameter of xylenes and allows *para*-xylene yield to be increased by diffusion shape selectivity during the isomerization of *meta*-xylene [13].

Over the past decade, numerous new zeolite structures and compositions that present quite unique pore topologies have been studied [14–23]. Among these, there is a material named ITQ-13 [24] with a unique pore topology formed by 9-MR channels intersected by perpendicular 10-MR channels with pore diameter slightly smaller than that of ZSM-5 zeolite [25]. It appears to us that such a zeolite may be of interest as an m-xylene isomerization catalyst, because the size of the channels may introduce a further discrimination among the different xylene isomers. Furthermore, it will be of interest to determine whether the 9-MR channel can play an active role in the diffusion of any of the isomers.

To investigate this, we carried out atomistic molecular dynamics for studying the diffusion of the xylene isomers and catalytic experiments that show the influence of pore dimensions and topology on product distribution in ITQ-13. We compare the results with those obtained with ZSM-5, NU-87, and β to rationalize the interesting behavior of the ITQ-13 material.

* Corresponding author.
E-mail address: acorma@itq.upv.es (A. Corma).

0021-9517/$ – see front matter
doi:10.1016/j.jcat.2006.05.034

2. Experimental

2.1. Molecular dynamics technique

Atomistic molecular dynamics (md) calculations were performed to simulate the diffusion of *ortho*-xylene, *para*-xylene, and 1,2,4-trimethylbenzene in purely siliceous ITQ-13. The md simulations were carried out using the general purpose DL_POLY_2.13 code [26]. Timesteps of 1 fs and an equilibration temperature of 650 K were used. The pure silica zeolitic system comprises 1344 atoms to which parallelepiped periodic boundary conditions are applied. A unique loading of 10 aromatic molecules is modeled with the same periodic boundary conditions applied to the sorbates in the zeolite. Runs of 500 ps were carried out within a NVE ensemble at 650 K. Three simulations with pure sorbate (one each *ortho*-xylene, *para*-xylene, and 1,2,4-trimethylbenzene) were considered. Full motion of the framework atoms was considered throughout the simulations. The following expression was used to calculate the MSD plots [27]:

$$\left\langle X^2(t)\right\rangle = 1/(N_{\mathrm{m}}N_{\mathrm{to}})\sum_i\sum_{t_{\mathrm{o}}}\left[X_i(t+t_{\mathrm{o}})-X_i(t_{\mathrm{o}})\right]^2, \tag{1}$$

where N_{m} is the number of diffusing molecules, N_{to} is the number of time origins used in calculating the average, and X_i is the coordinate of the center of mass of molecule i.

The diffusion coefficients are then calculated from the Einstein relation,

$$\left\langle X^2(t)\right\rangle = 6Dt + B, \tag{2}$$

where t is the simulation time and B is the thermal factor arising from atomic vibrations. The activation energy for the diffusion is calculated according to Arrhenius-type equation

$$D = D_0\exp(-E_{\mathrm{a}}/RT). \tag{3}$$

2.2. Interatomic potentials

Four terms are needed to model this system:

$$V_{\mathrm{total}} = V_{\mathrm{zeolite}} + V_{\mathrm{organic}} + V_{\mathrm{organic\text{–}organic}} + V_{\mathrm{zeolite\text{–}organic}}. \tag{4}$$

The potential for the framework, V_{zeolite}, was originally derived by Catlow et al. [28] and is essentially a Born model potential comprising three terms,

$$V_{\mathrm{zeolite}} = V_{\mathrm{buck}} + V_{\mathrm{three\text{-}body}} + V_{\mathrm{coul}}. \tag{5}$$

The potential for the sorbate, V_{organic}, comprises four terms and was taken from Oie et al. [29],

$$V_{\mathrm{organic}} = V_{\mathrm{two\text{-}body}} + V_{\mathrm{three\text{-}body}} + V_{\mathrm{four\text{-}body}} + V_{\mathrm{coul}}. \tag{6}$$

All of the parameters used and more details of the methodology are given in a previous study [12].

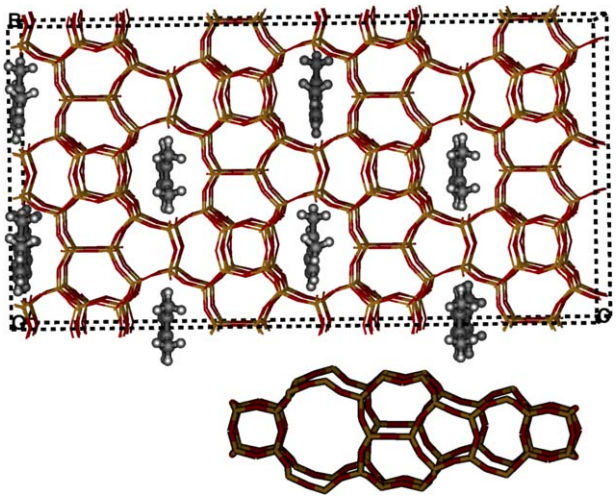

Fig. 1. View of the 2 × 2 × 2 unit cell of ITQ-13 and 10 molecules of *ortho*-xylene used in one of the molecular dynamics runs. The 9 MR can be seen (parallel to [100]), and the 10 MR are parallel to [010]. The large cavities (shown at the bottom) are terminated (left and right) by double four ring (D4R) units.

2.3. Structural data

ITQ-13 (ITH) [30] is a zeolite with a channel system formed by 9- and 10-MR pores. The 9-MR channels with dimensions 4.0 × 4.8 Å run parallel to [100], and the 10-MR channel, with dimensions 4.8 × 5.1 Å, is parallel to [010] (see Fig. 1). These two channels are interconnected, by means of a larger void space that run parallel to [001] with a 10-MR cross-section of dimensions 4.8 × 5.3 Å. Those cavities are 15.5 Å long and are terminated by double four-ring units (D4R) at both ends (Fig. 1). The three microporous voids are interconnected and together compose a unique diffusional environment that could be of interest for reactions carried out commercially with 10-MR zeolites, as catalytic cracking results show [31]. ZSM-5 [32], with code MFI [30], contains interconnected channels of 10 MR parallel to [100] (5.1 × 5.5 Å) and to [010] (5.3 × 5.6 Å). In this sense, ZSM-5 is known to be able to discriminate among the different xylene isomers by the different rate of diffusion, particularly in the case of *para*- and *ortho*-xylene. Thus, we first studied, by molecular dynamics, the diffusion of aromatics through the 10- and 9-MR channels of ITQ-13 and through the 10-MR channels of ZSM-5.

NU-87 [33] (International Zeolite Association code NES [30]) is a zeolite-containing channel system with 10 and 12 MRs. The 12 MRs are parallel to [001] and form the cross-section of a large cavity with a cross-section formed by 12 MRs of dimensions 5.3 × 6.8 Å. Perpendicular to these windows, across [101], a 10-MR channel system exits with dimensions 4.8 × 5.7 Å. β zeolite [34] (code BEA [30]) has two connected 12-MR channel systems with dimensions 6.6 × 6.7 Å (parallel to [100] and [010]) and 5.6 × 5.6 Å (parallel to [001]).

2.4. Materials

ITQ-13 samples were synthesized following two procedures reported previously [24,25], the first obtained by a postsynthe-

Table 1
Characteristic of samples used in this work

Sample	ZSM-5-(20)[a]	ZSM-5-(40)	ITQ-13-A	ITQ-13-B	NU-87[a]	Beta-A[a]	Beta-B
Ref.	CBV5020	CBV8020					
(Si + Ge)/Al ratio	20	40	80	50	17	13	50
Si/Ge ratio	–	–	–	15	–	–	16
Crystal size	0.1	0.5–1	0.5–1.5	0.2–0.3	0.3–0.4	0.17	0.5
S (BET) (m^2/g)	379	386		367	390	457	510
Brönsted acidity (μmol Py/g)							
$T = 423$ K		113	45	63			
$T = 523$ K	163	92	36	55	155	104	80
$T = 623$ K	112	44	13	28	108	62	23
Lewis acidity (μmol Py/g)							
$T = 423$ K		23	103	48			
$T = 523$ K	11	17	100	32	25	7	13
$T = 623$ K	9	13	85	27	13	5	12

Note. Crystal size estimated from SEM pictures. Acid strength distribution determined by IR-pyridine measurements at different desorption temperatures, using the extinction coefficients given by Emeis [35].
[a] Ref. [12].

sis lattice replacement of Al by B and the second when Ge is present in the synthesis gel. β zeolite was prepared in our laboratory using a similar procedure, adding the appropriate amount of Ge in the gel. NU-87 was synthesized as described previously [33]. ZSM-5 samples (CBV 5020 and CBV8020) were provided by Zeolyst.

The Si/Al and Si/Ge ratios were determined by chemical analysis. Porosity was determined by nitrogen adsorption at 77 K. The acidic properties were characterized by pyridine adsorption followed by desorption at increasing temperatures (423/523/623 K). The concentration of Brönsted and Lewis acid sites was determined from the IR spectrum after each desorption step, by the area of the IR bands at ca. 1550 (IA_B) and 1450 cm^{-1} (IA_L), applying the equations of Emeis [35],

$$C_B = 1.88\, IA_B R^2 / W \tag{7}$$

and

$$C_L = 1.42\, IA_L R^2 / W, \tag{8}$$

where B represents the Brönsted acid center, L represents the Lewis acid center, C is concentration (mmol/g catalyst), IA is integrated absorbance (cm^{-1}), R is the radius of the catalyst disk (cm), and W is the weight of the disk (mg).

Surface area measurements were obtained by the standard BET method. The average crystallite size of the zeolites was determined by scanning electron microscopy (SEM). The physicochemical properties of catalytic materials are given in Table 1. All samples were calcined at 823 K for 6 h under air flow before use.

2.5. Reaction procedure

Catalytic experiments were conducted in vapor phase at atmospheric pressure in a fixed-bed continuous glass down-flow reactor (11 mm i.d.). The catalyst (with particle size within the range 0.3–0.5 mm to avoid intraparticle diffusion limitations) was diluted with glass to maintain a constant bed volume.

The process was carried out with a *meta*-xylene/N_2 molar ratio of 0.25. Before reactant was added, the catalyst was heated at 623 K at a heating rate of 5 K/min, under a flow of nitrogen. After 30 min, the temperature was raised to 723 K and kept at that temperature for 1 h. The reactor was then cooled to reaction temperature, 623 K for *meta*-xylene isomerization. When the temperature was stabilized, the reactant was fed at the top of the reactor. Reaction products were taken at 10, 30, 60, 180, and 360 s and analyzed in a gas chromatograph (HP5890II) equipped with a Supelco-WAX10 capillary column (60 m long, 0.2 mm i.d.) and a flame ionization detector (FID).

Preliminary experiments were done to establish the conditions for which no control by external or internal diffusion exists. Because the catalytic activity of the different zeolites differed substantially, the amount of catalyst in the reactor and the molar flow of reactants were adapted to obtain the desired degree of conversion. Initial selectivities were obtained from the initial rates of formation of the products. Initial conversions, X_0, and yields (not influenced by catalyst deactivation) were calculated by extrapolating the conversion X, measured at different times on stream (t) according to the following equation:

$$X = X_0 \exp(-kt^{1/2}). \tag{9}$$

3. Results and discussion

3.1. Molecular dynamics simulations

The diffusion path in the 10-MR channels of ITQ-13 are given in Figs. 2–8. More specifically, Figs. 2–5 show the diffusion through the 10-MR channel parallel to [010] and inside the larger void space parallel to [001]. It is clear that although *para*-xylene diffuses through both of them, larger diffusional paths are observed across the 10-MR channel (Fig. 2). Diffusion of *para*-xylene through the larger void space is characterized by paths across the vertical axis in Fig. 2, for example, the corresponding to $y = -10$ Å and $z \geqslant 10$ Å. In the case of *ortho*-xylene (Fig. 3), *meta*-xylene (Fig. 4), and 1,2,4-

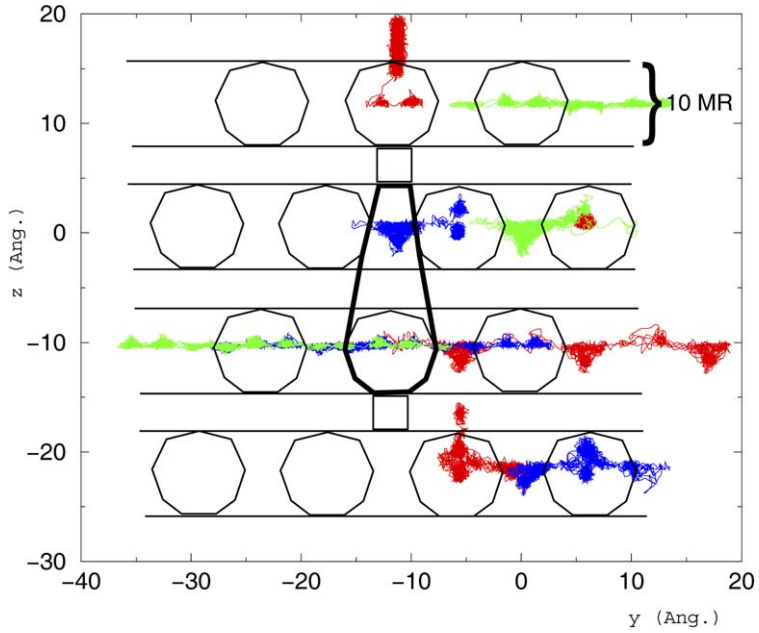

Fig. 2. Trajectories of the 10 *para*-xylene molecules in ITQ-13 at 650 K. The axes shown are z and y (vertical and horizontal, respectively). The 10-MR channels run parallel to the y axis, whereas the 9-MR channels are perpendicular to the yz plane. The large cavities (one of them is highlighted) allow some diffusion through the z direction and these cavities are accessible through one 9-MR window and two 10-MR windows.

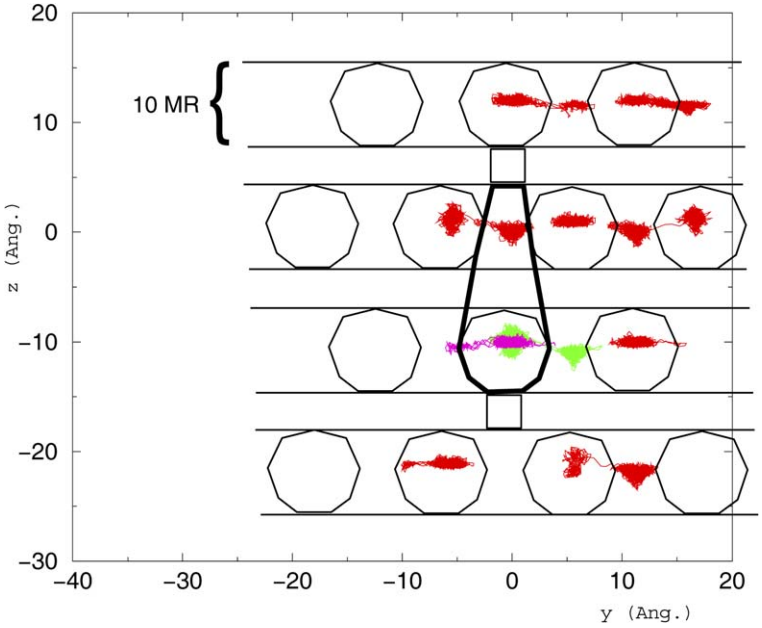

Fig. 3. Trajectories of the 10 *ortho*-xylene molecules in ITQ-13 at 650 K. The axes shown are z and y (vertical and horizontal, respectively). The 10-MR channels run parallel to the y axis, whereas the 9-MR channels are perpendicular to the yz plane. The large cavities (one is highlighted) allow some diffusion through the z direction and these cavities are accessible through one 9-MR window and two 10-MR windows.

trimethylbenzene (Fig. 5), the trajectories are similar and the diffusion is more restricted than for *para*-xylene. In the case of the larger void space, diffusion is restricted around the positions of minimum energy, and molecules do not show a large diffusional path.

In the case of the 9-MR channel, the diffusion of *para*-xylene (Fig. 6) is possible, with a few events observed, but it is much more restricted than in the 10-MR channel. On the other hand, *ortho*-xylene (Fig. 7), *meta*-xylene (not shown), and 1,2,4-trimethylbenzene (Fig. 8) do not even enter the 9 MR due to severe size restrictions, and consequently this smaller channel system is of little use for diffusing xylenes (even *para*-xylene).

The diffusion coefficients obtained from the mean square displacements (Fig. 9) show a considerable faster diffusion of *para*-xylene with respect to the other xylene isomers and trimethylbenzene (Table 2). It is very interesting to observe that the diffusion results are very different for ITQ-13 and ZSM-5

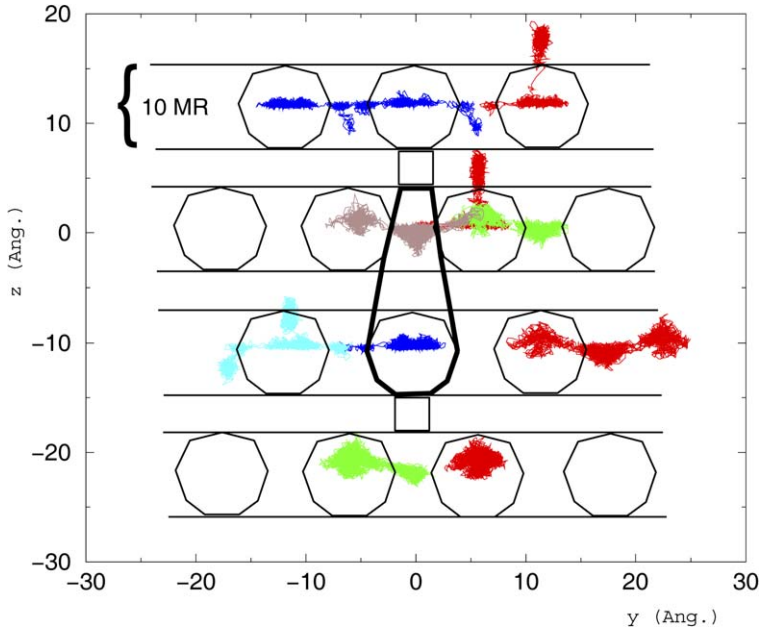

Fig. 4. Trajectories of the 10 *meta*-xylene molecules in ITQ-13 at 650 K. The axes shown are z and y (vertical and horizontal, respectively). The 10-MR channels run parallel to the y axis, whereas the 9-MR channels are perpendicular to the yz plane. The large cavities (one is highlighted) allow some diffusion through the z direction and these cavities are accessible through one 9-MR window and two 10-MR windows.

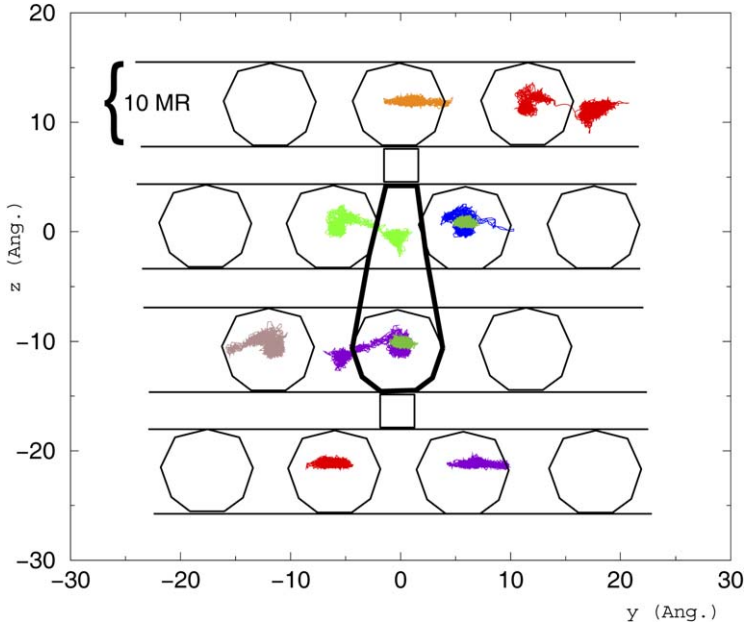

Fig. 5. Trajectories of the 10 1,2,4-trimethylbenzene molecules in ITQ-13 at 650 K. The axes shown are z and y (vertical and horizontal, respectively). The 10-MR channels run parallel to the y axis, whereas the 9-MR channels are perpendicular to the yz plane. The large cavities (one is highlighted) allow some diffusion through the z direction and these cavities are accessible through one 9-MR window and two 10-MR windows.

(Table 2), despite the fact that in both cases diffusion occurs through 10-MR pores. We can see two reasons for this finding: the smaller pore dimensions of ITQ-13, and the fact that in the ITQ-13, the 10-MR channels are connected through the larger void space of 15.5 Å. The presence of these larger void spaces will negatively influence the diffusion. Indeed, when the molecule diffuses through the 10-MR channel in ITQ-13 and diverts into the large cavity, this acts as a diffusional trap in which the molecule experiences an extensive local motion that retards a new jump back into the 10-MR channel, where the diffusion is considerably faster.

To further elaborate on the effect on molecular diffusion introduced by the presence of those cavities, we compared the diffusion coefficients of *para*- and *ortho*-xylene, as well as 1,2,4-trimethylbenzene, in NU-87. The structure of this zeolite [30] is formed by a system of 10-MR channels connected through a 12 MR "cage." The effect of this 12-MR connecting "cage" will entrap the molecules, decreasing the diffusion

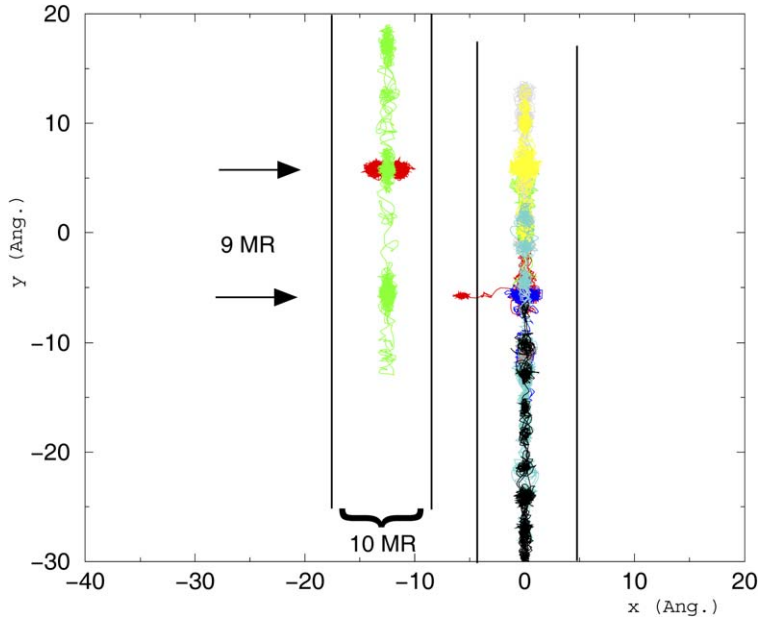

Fig. 6. Trajectories of the 10 *para*-xylene molecules in ITQ-13 at 650 K. The axes shown are y and x (vertical and horizontal, respectively). The 10-MR channels run parallel to the y axis, whereas the 9-MR channels run parallel to the x axis.

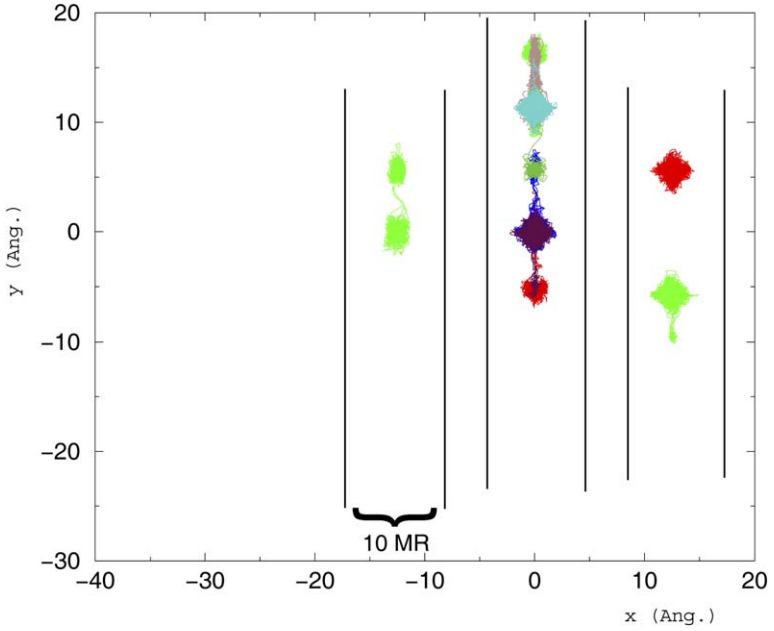

Fig. 7. Trajectories of the 10 *ortho*-xylene molecules in ITQ-13 at 650 K. The axes shown are y and x (vertical and horizontal, respectively). The 10-MR channels run parallel to the y axis, whereas the 9-MR channels run parallel to the x axis.

coefficient. Indeed, the results in Table 2 demonstrate that the diffusion coefficients in ITQ-13 and NU-87 are very similar despite the differences in topology. However, we should take into account that the pore diameters of the 10-MR channels are similar in these two zeolites. Therefore, the role of the pore diameter of ITQ-13 must be studied independently of the presence of cavities.

We have done this by first generating an hypothetical zeolite (with a correct topology, connectivity, and structural features) containing a single channel system composed of 10 MRs of the same size and shape as the 10-MR channel of ITQ-13. We then introduced *para*-xylene into this hypothetical structure in the same concentration as in the corresponding simulation of *para*-xylene in ITQ-13, and performed a fixed framework molecular dynamics run with the same technique and conditions as in the previous runs. The results show very low diffusivity of *para*-xylene, with a diffusion coefficient of 0.6×10^{-6} cm^2/s, indicating that the diffusivity of *para*-xylene in a straight channel of 10 MRs, similar to that of ITQ-13 but without intersects from both the 9 MR, and that the larger void space is very low. Therefore, the diffusivity of *para*-xylene in ITQ-13 is due mainly to the supercages that intersect the 10 MRs and not to

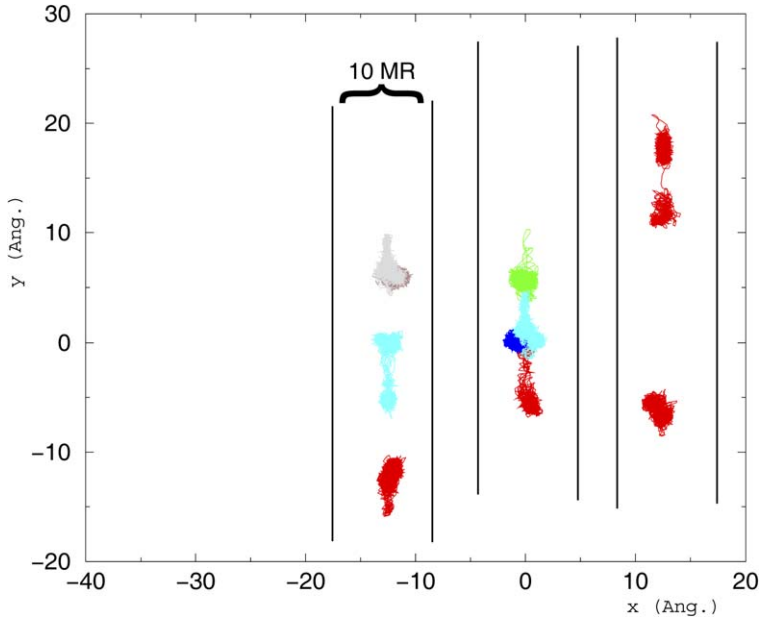

Fig. 8. Trajectories of the 10 1,2,4-trimethylbenzene molecules in ITQ-13 at 650 K. The axes shown are y and x (vertical and horizontal, respectively). The 10-MR channels run parallel to the y axis, whereas the 9-MR channels run parallel to the x axis.

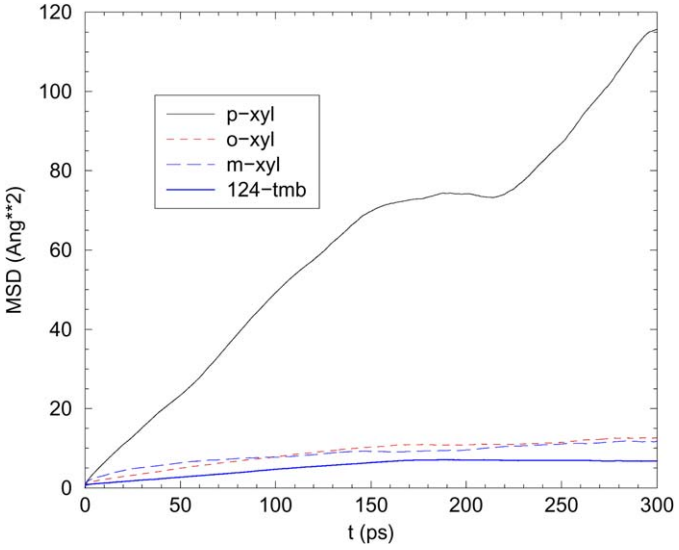

Fig. 9. Mean square displacements obtained from the trajectories of *para*-, *meta*-, *ortho*-xylene and 1,2,4-trimethylbenzene in ITQ-13 at 650 K.

the 10-MR windows, which are of limited size compared to other 10-MR channels. Larger void spaces that intersect channels sometimes may act as molecular traps (which decrease the diffusivity) when channels are wide enough, but larger void spaces may increase diffusivity when the channels are very narrow so as to allow molecular passage. In this case, the channels act by increasing the free diameter available for the molecular diffusivity. This latter effect is what we observe for *para*-xylene in the 10-MR channels of ITQ-13; the channels alone (as computed for the hypothetical structure) are too narrow (as the aforementioned low diffusivity indicates), but the 10-MR channels intersected by larger void spaces (as present in the ITQ-13 structure) provide sufficient room for the *para*-xylene molecules to diffuse.

Table 2
Diffusion coefficients from molecular dynamics simulations at 650 K

Sorbate in zeolite	Loading[a]	D[b]	Reference
Ortho-xylene in NU-87	0.017	1.42	[12]
Para-xylene in NU-87	0.017	8.30	[12]
1,2,4-trimethylbenzene in NU-87	0.017	0.95	[12]
Ortho-xylene in β	0.021	41.29	This study
Meta-xylene in β	0.021	53.32	This study
Para-xylene in β	0.021	87.02	This study
1,2,4-trimethylbenzene in β	0.021	18.44	[12]
Ortho-xylene in ZSM-5	0.026	5.54	[12]
Meta-xylene in ZSM-5	0.026	1.38	This study
Para-xylene in ZSM-5	0.026	40.76	[12]
1,2,4-trimethylbenzene in ZSM-5	0.026	1.81	[12]
Ortho-xylene in SSZ-33	0.036	4.99	[12]
Para-xylene in SSZ-33	0.036	11.36	[12]
1,2,4-trimethylbenzene in SSZ-33	0.036	2.53	[12]
Ortho-xylene in ITQ-13	0.022	0.65	This study
Meta-xylene in ITQ-13	0.022	0.54	This study
Para-xylene in ITQ-13	0.022	5.78	This study
1,2,4-trimethylbenzene in ITQ-13	0.022	0.27	This study

[a] Organic molecules per SiO_2.
[b] Diffusion coefficient (10^{-6} cm^2/s).

In conclusion, and from the theoretical work, we have seen that xylenes diffuse more slowly in ITQ-13 than in ZSM-5. However, the *para*/*ortho* diffusivity ratio is similar for both zeolites. Taking these parameters into account, we can predict for the former zeolite a similar sieving effect among *para*- and *ortho*-xylene as in ZSM-5, with the corresponding shape selectivity for *para*-xylene. However, we can also expect that the presence of a large cavity in ITQ-13 should favor equilibration of the isomers within the cavity, which will result in a decrease of the *para*-xylene-to-*ortho*-xylene ratio. Furthermore, the slower diffusivity in ITQ-13 may also imply a greater contribution of the active sites located at the external surface

Table 3
Diffusion coefficients of *meta*-xylene in ITQ-13 at different temperatures

Sorbate in zeolite	Loading[a]	D[b]	Temperature (K)
Meta-xylene in ITQ-13	0.022	0.54	650
Meta-xylene in ITQ-13	0.022	2.02	700
Meta-xylene in ITQ-13	0.022	3.94	750

[a] Organic molecules per SiO_2.
[b] Diffusion coefficient (10^{-6} cm^2/s).

Table 4
Conversion and product distribution in *meta*-xylene isomerization and disproportionation over ITQ-13, ZSM-5, NU-87, and Beta samples

Sample	ZSM-5-(40)	ITQ-13-B	NU-87[c]	Beta-B
Weight catalysts (mg)	95.9	75.8	20.3	51.0
WHSV (min^{-1})	3.6	3.1	21.4	3.4
Meta-xylene conversion (mol%)[a]	21.1	22.8	26.9	22.1
Yield in products				
Isomerization	20.7	22.2	19.1	16.0
Disproportionation	0.4	0.6	7.8	6.1
Products distribution (%)[b]				
Toluene	1.4	1.3	14.9	14.1
Para-xylene	66.8	53.1	39.7	39.6
Ortho-xylene	31.4	44.6	31.3	32.8
1,3,5-TMB	0.0	0.0	0.3	3.7
1,2,4-TMB	0.3	1.1	13.0	8.8
1,2,3-TMB	0.0	0.0	0.7	1.1
Normalized distribution of trimethylbenzenes (TMB) (%)				
1,3,5-TMB	0.0	0.0	2.3	27.0
1,2,4-TMB	100.0	100.0	92.5	64.7
1,2,3-TMB	0.0	0.0	5.2	8.3

Note. Reaction conditions: *meta*-xylene-to-N_2 molar ratio, 4; temperature 623 K.
[a] *Meta*-xylene conversion obtained at 0 s time-on-stream.
[b] *Meta*-xylene free.
[c] Ref. [12].

versus those located at the internal surface. Therefore, when all of the parameters are taken into account, we could expect a lower *para*-xylene to *ortho*-xylene ratio and a smaller isomerization to disproportionation ratio in the case of ITQ-13.

3.2. Effect of temperature on the diffusion of meta-xylene in ITQ-13

The variation of the diffusion coefficients at different temperatures can give us the activation energy of the process according to (3). The diffusion of *meta*-xylene in ITQ-13 has been calculated at 650, 700, and 750 K, and the corresponding diffusion coefficients are shown in Table 3. With the data from the table, the activation energy obtained is 19.4 kcal/mol, which corresponds to an activated molecular diffusion.

3.3. Catalytic behavior

Catalytic results for the isomerization and disproportionation of m-xylene in the zeolites used in this study are given in Table 4. The isomerization and disproportionation of m-xylene has been proposed as a test reaction that allows to differentiate between 10-MR and 12-MR pore zeolites, while being sensitive

Table 5
Para/*ortho* ratio (p/o), isomerization/disproportionation ratio (i/d), and distribution of trimethylbenzenes at low conversions of m-xylene on different zeolites

Zeolite	X_o (% mol)	p/o	i/d	Trimethylbenzene (% normalized)			1,2,3/1,3,5 ratio
				1,3,5	1,2,4	1,2,3	
ZSM-5-(20)[a]	11.0	2.3	34.3	–	100	–	–
	26.7	2.0	34.1	4.4	91.8	3.8	0.87
ZSM-5-(40)	21.1	2.1	55.0	–	100	–	–
	23.5	1.9	56.0	–	100	–	–
	27.3	1.9	45.7	–	100	–	–
ITQ-13-A	3.8	1.4	45.6	–	100	–	–
	8.6	1.3	38.5	4.4	95.6	–	–
	19.2	1.3	40.2	9.7	90.3	–	–
ITQ-13-B	19.5	1.2	42.9	–	100	–	–
	22.8	1.2	41.7	–	100	–	–
	25.9	1.3	32.1	6.0	90.7	3.3	0.57
NU-87[a]	26.9	1.3	3.4	2.4	92.5	5.1	2.2
	30.7	1.3	2.4	1.6	93.3	5.1	3.1
Beta-A[a]	19.2	1.1	2.9	26.4	65.8	7.9	0.30
	34.8	1.1	2.3	27.3	64.4	8.3	0.30
Beta-B	10.8	1.1	3.0	26.7	65.8	7.5	0.28
	22.1	1.2	2.6	27.0	64.7	8.3	0.31
Equilibrium (623 K)		1.0		24.0	68.0	8.0	0.33

[a] Ref. [12].

to the presence of lobes, cages, or crossing channels [36–43]. This is so because during the isomerization of m-xylene, both *para*-xylene and *ortho*-xylene are formed and, at low levels of conversion, 10-MR zeolites give a higher *para*/*ortho* (p/o) ratio than 12-MR zeolites. This was rationalized in terms of differences in the diffusion of both isomers through the narrower channels of the 10-MR zeolites. Moreover, the disproportionation of xylenes to give trimethylbenzenes and toluene is a bimolecular reaction involving a much bulkier transition state than the monomolecular isomerization process. It is clear that the ratio of isomerization to disproportionation (i/d), and the distribution of trimethylbenzenes will give an indication on the presence of lobes, cavities, or crossing channels where the available space will be large enough to allow bimolecular reactions. In addition to the information on the topology of zeolites, the isomerization of m-xylene, when performed at the experimental conditions described above, will indicate the potentiality of a zeolite for the industrial isomerization of C_8 alkylaromatic m-xylene-rich fraction.

The results obtained with samples ZSM-5-(40) and ITQ-13-B, both with similar Si/Al ratios (see Table 1), show isomerization-to-disproportionation ratios (Table 5) much higher than those obtained with 12-MR zeolites or amorphous silica–alumina [44]. Furthermore, the p/o ratio in the products was analyzed at different levels of conversion (Fig. 10), demonstrating that the values are higher than expected based on the thermodynamic equilibrium (1.05). Combining these results with the fact that the catalytic activity of both zeolites is similar (Table 4), we conclude that an important fraction of the reaction occurs within the pores of the ITQ-13. Nevertheless, it should be taken into account that the crystallite size of ITQ-13 is smaller than

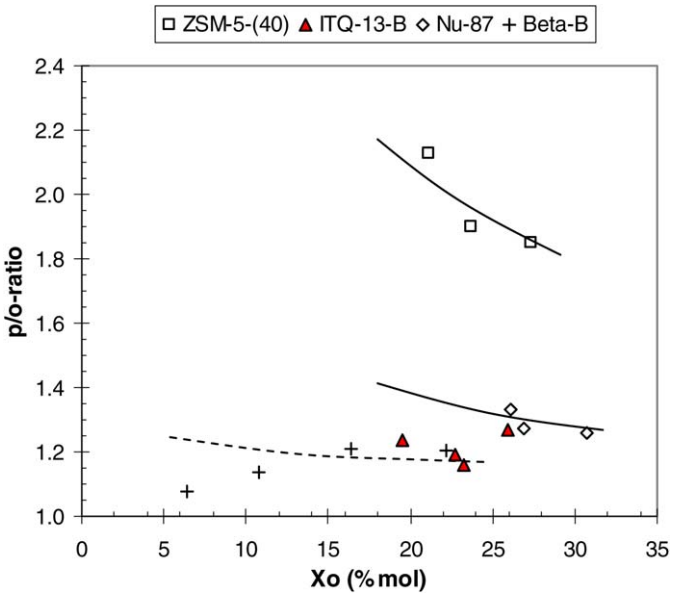

Fig. 10. *Para*/*ortho* ratio of xylene isomers, over ZSM-5-(40), ITQ-13B, NU-87, and Beta-B zeolites versus initial conversion in the isomerization of *meta*-xylene, at 623 K and 0.2 atm partial pressure.

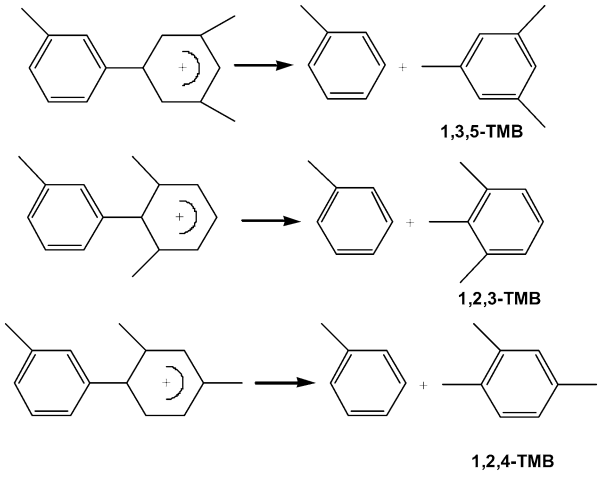

Fig. 11. Intermediates and products of the xylene disproportionation.

Table 6
Molecular docking performed by optimizing the orientation of each of the TMB isomers (1,2,3-TMB, 1,2,4-TMB, and 1,3,5-TMB) in two locations of the ITQ-13 large cavity

Sorbate in ITQ-13 cavity	Energy of interaction sorbate–cavity (kcal/mol)	
	Middle	Intersection
1,2,3-TMB	24	−8
1,2,4-TMB	9	−2
1,3,5-TMB	29	−8

Note. The location called 'middle' is inside the cavity, where the molecule is surrounded by a 10 MR (4.8 × 5.3 Å). The location called 'intersection' corresponds to the intersection between the large cavity and the 9-MR channels. Both locations can be easily guessed from the large cavity depicted in Fig. 1. The result of the molecular docking is the short range van der Waals interaction energy between the TMB molecule and the zeolite cavity. The sorbates are shown in Fig. 11.

that of ZSM-5, and, consequently, a greater contribution of the external surface to the global catalysis can be expected in the former with the corresponding decrease of the p/o and i/d ratio. However, we also cannot neglect the fact that the presence of the large cavity in ITQ-13 should also contribute to the equilibration of the isomers there and, consequently, may have a negative impact on the p/o ratio observed. In fact, comparing the results obtained with the two ZSM-5 samples with different crystallite sizes (Table 5), despite their differences in framework Si/Al ratio, the influence of crystallite size (and thus the external surface-to-internal surface ratio) in the range that we are comparing here has a minor effect on the p/o ratio. Taking this result into consideration, we can also say that the differences in p/o ratio observed between ZSM-5 and ITQ-13 are so large that another factor besides differences in crystallite size should play an important role on the selectivity observed. We believe that, in agreement with the impact of the internal cavities of ITQ-13 on the diffusion coefficients obtained by molecular dynamics calculations, this should be the main reason accounting for the lower-than-expected p/o ratio observed with ITQ-13.

An additional selectivity parameter can provide information on the role of internal cages: the distribution of trimethylbenzenes formed by disproportionation of m-xylene. Indeed, this reaction occurs through the formation of three possible 1,1-diphenylmethane transition states leading to 1,2,4-, 1,3,5-, and 1,2,3-trimethylbenzene (TMB) isomers (Fig. 11). None of the three transition state complexes can be easily accommodated in the pores of 10-MR zeolites. Then, when small disproportionation occurs, the less impeded complex that leads to the formation of 1,2,4-TMB should be favored, provided that there is no important contribution of the external surface activity to disproportionation.

Results presented in Table 4 clearly show that in ZSM-5, as well as in ITQ-13, the only TMB isomer detected was the 1,2,4-TMB. In the case of ITQ-13, one would expect the 15.5-Å-long cavities to accommodate any of the three 1,1-diphenylmethane transition states. To check this, a docking simulation was performed; the three TMB isomers were located, and their orientation was optimized in two locations of the large cages of ITQ-13. The first location considered is the middle of the cavity; the second is the intersection with the 9-MR channel. The results given in Table 6 show that only 1,2,4-TMB can fit in the large cavity. Nonetheless, the three isomers can fit in the intersection space, but once formed, only 1,2,4-TMB is expected to diffuse out of the large cavity, whereas the other isomers (1,2,3-TMB and 1,3,5-TMB), if formed, should isomerize to 1,2,4-TMB, so that diffusion is allowed. Thus, despite the possible formation of the three TMB isomers inside the pore system of ITQ-13, that only the 1,2,4-TMB is observed can be due to the impossibility of 1,2,3- and 1,3,5-TMB isomers diffusing out through the pores. This could be the case because the kinetic diameter of the 1,2,4-TMB (5.5 × 6.7 Å) is less than that of the other two isomers (5.9 × 6.6 Å), and diffusion calculations already give a very low diffusion coefficient for 1,2,4-TMB in ITQ-13.

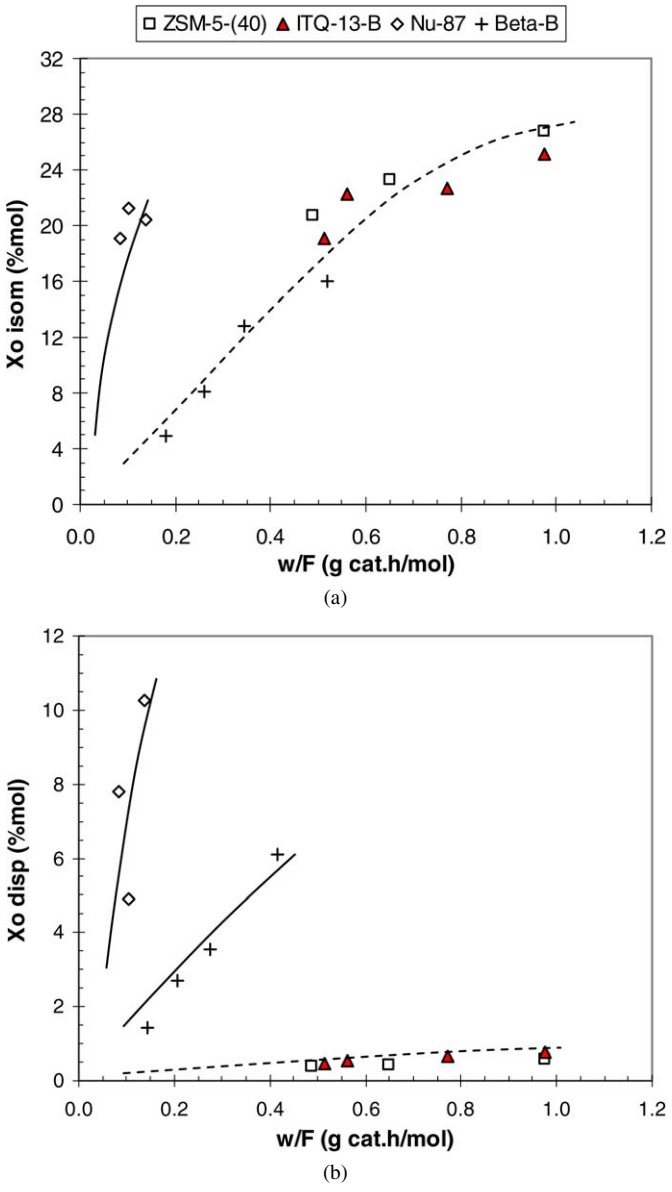

Fig. 12. Initial conversion in the isomerization (a) and disproportionation (b) of *meta*-xylene at 623 K and 0.2 atm partial pressure, over ZSM-5-(40), ITQ-13B, NU-87, and Beta-B zeolites versus cat/oil (w/F—g of catalyst × h/mol m-xylene in feed).

Because the 10-MR pore dimensions of ITQ-13 are very similar to those of NU-87, as are the calculated diffusion coefficients for xylenes and 1,2,4-TMB with the two zeolites, we also performed isomerization of m-xylene with NU-87 and β zeolites. The activity of the NU-87 (Fig. 12) is greater than that of the other samples; this difference in activity can be explained based on the difference in the framework Si/Al and number and strength of acid sites (Table 1). Indeed, the amount of the stronger Brönsted acid sites needed to perform *meta*-xylene isomerization and disproportionation, which corresponds to those retaining pyridine at 623 K desorption temperature, is greater in NU-87 [45].

With respect to the i/d ratio, small but significant differences exist. At the same level of total conversion, ITQ-13 always gives an i/d ratio greater than that of NU-87 or β zeolites and similar to that of ZSM-5. The presence of larger void spaces in the former zeolite, which give time and space for m-xylene to react, leads to low disproportionation.

Table 4 compares the distribution of the trimethylbenzenes obtained with zeolite ITQ-13 at different *meta*-xylene conversion levels with that obtained with ZSM-5, NU-87, and β zeolites. The table shows that 1,2,4-TMB is initially formed with ITQ-13 in larger amounts than in β zeolite and above the thermodynamic equilibrium, whereas 1,3,5- and 1,2,3-TMB are formed in lower amounts than those predicted by the thermodynamic equilibrium. The analysis of these results indicates that the less bulky bimolecular transition state (1,2,4-TMB) is clearly favored in the case of ITQ-13 and is the only one allowed to diffuse out of the zeolite.

The ratio of the initial selectivities for 1,2,3- to 1,3,5-TMB obtained at low levels of disproportionation (Table 5) seems to reflect the shape of the pores. The ratio is lower in lobate pores (FAU or L zeolites) than in zeolites in which the configuration of the side pockets and side channels does not create regular lobes (OFF, MOR, Omega) [39]. In straight pores with side pockets at regular distances the 1,2,3-TMB-to-1,3,5-TMB ratio is initially high, whereas for 12-MR zeolites consisting of alternating cages or lobes separated by 12 MRs, this ratio is much lower. The ratio of those trimethylbenzene isomers for zeolite NU-87 (Table 5), is higher than for β zeolite, indicating that the reactants see smaller void spaces in NU-87 than in β. It should be taken into account that these results are not masked by reaction at the external surface, because the crystallite size of the samples is very similar for ITQ-13, NU-87, and β, and in any case is larger for ZSM-5-(40) than for ITQ13-B (Table 1).

Regarding the influence of the acidity, measured through either the Si/Al ratio or the pyridine adsorbed (Table 1), it correlates with the activity. Fig. 12 shows that the order of activity relates to the order of acidity as in NU-87 > ZSM-5-(40) $\geqslant$ ITQ-13B $\cong$ Beta-B. Likewise, Fig. 13 shows that the ITQ-13A (with Si/Al = 80) is the least active, followed by ITQ-13B and ZSM-5-(40) (with Si/Al = 40–50), and then the most acidic ZSM-5-(20) (with Si/Al = 20) the most acidic.

The variation of the selectivity of the reaction (p/o-xylene ratio) with conversion (Fig. 14) shows two different trends that do not correlate with acidity or crystal size, but rather with microporosity factors. The presence of cavities in ITQ-13, which are not present in ZSM-5, allow a larger degree of isomerization, and this decreases the p/o-xylene ratio in ITQ-13 with respect to ZSM-5.

4. Conclusion

We have studied the diffusion of xylenes and trimethylbenzenes in the pore topology of ITQ-13 zeolite via simulation methods. In the case of the 9-MR channel, the diffusion of *para*-xylene is possible, with a few events observed, but it is much more restricted than in the 10-MR channel. On the other hand, *ortho*-xylene, *meta*-xylene, and 1,2,4-trimethylbenzene do not even enter the 9 MRs due to severe size restrictions, and, consequently, this smaller channel system is of little use for diffusing xylenes.

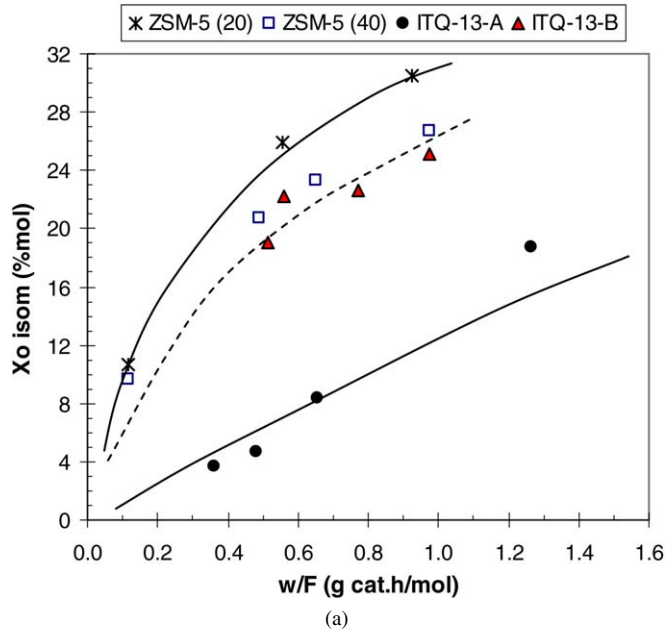

(a)

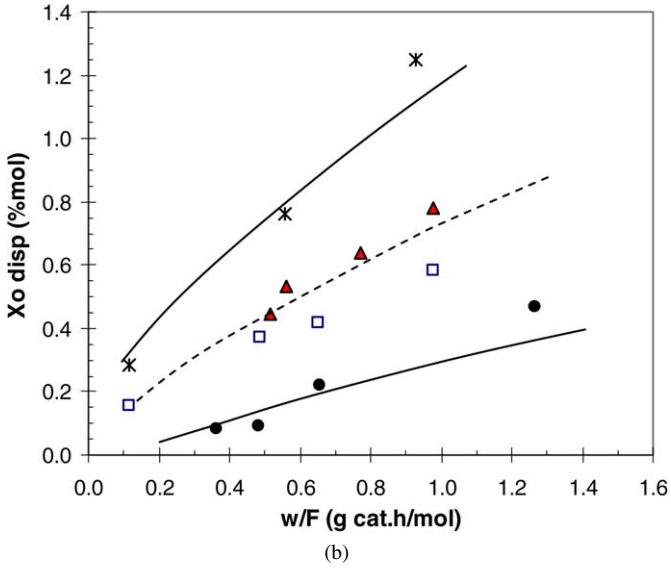

(b)

Fig. 13. Initial conversion in the isomerization (a) and disproportionation (b) of *meta*-xylene at 623 K and 0.2 atm partial pressure, over ZSM-5-(20), ZSM-5-(40), ITQ-13-A, ITQ-13-B samples versus cat/oil (w/F—g of catalyst × h/mol m-xylene in feed).

Diffusion studies of *ortho*-xylene and *para*-xylene and 1,2,4-trimethylbenzene in ITQ-13 predict that whereas the three molecules can diffuse from one larger void space to another through the 10-MR channels, the diffusion coefficients should be similar as in a bidimensional 10-MR pore zeolite such as ZSM-5. This means that during *meta*-xylene isomerization, reactants and products formed by methyl shift isomerization or alkyl shift transalkylation will spend a considerable time within the ITQ-13 cavity, reacting further before intercavity migration occurs. This should drive the mixture toward thermodynamic equilibrium, neutralizing diffusion shape selectivity effects that will tend to enrich the gaseous stream with *para*-xylene.

The trimethylbenzenes product distribution observed and docking calculations indicate that 1,2,4-trimethylbenzene will

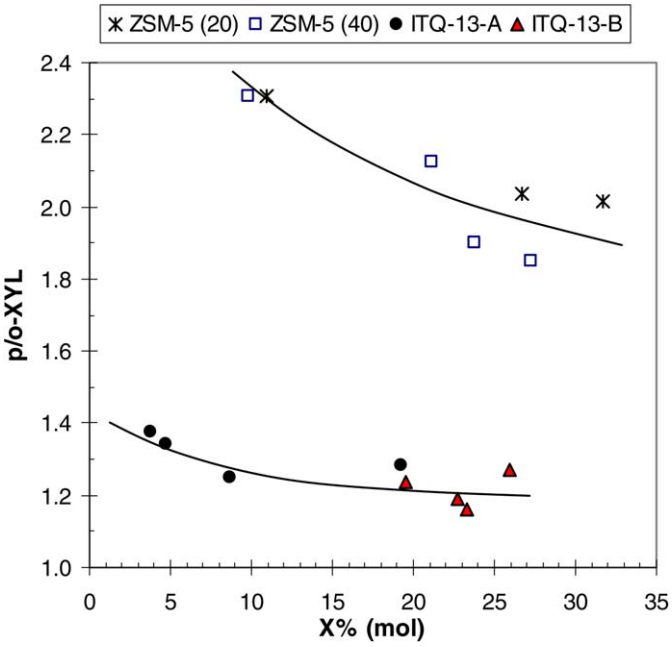

Fig. 14. *Para*/*ortho* ratio of xylene isomers, over ZSM-5-(20), ZSM-5-(40), ITQ-13-A, ITQ-13-B zeolites versus initial conversion in the isomerization of *meta*-xylene, at 623 K and 0.2 atm partial pressure.

be preferentially formed within the internal voids, but the two other isomers can also be formed at the intersections. However, isomers 1,2,3- and 1,3,5-trimethylbenzene cannot diffuse out through the pores and will isomerize to 1,2,4-trimethylbenzene, which is the only one that, although slowly, can diffuse out. With respect to the i/d ratio, ITQ-13 always gives a ratio higher than that of NU-87 or β zeolites and similar to that of ZSM-5.

Acknowledgments

We thank CIEMAT (Centro de Investigaciones Energeticas Medioambientales y Tecnologicas) for the use of their computational facilities. This work was supported by the Ministerio de Educacion y Ciencia of Spain through project MAT2003-07769-C02-01.

References

[1] P.B. Weisz, V.J. Frilette, J. Phys. Chem. 64 (1960) 382.
[2] S.M. Czicsery, ACS Monograph 171 (1976) 680.
[3] N.Y. Chen, W.E. Garwood, Catal. Rev. Sci. Eng. 28 (1986) 185.
[4] V.J. Frilette, W.O. Haag, R.M. Lago, J. Catal. 67 (1981) 218.
[5] N.Y. Chen, W.G. Darwood, F.G. Dwyer, Shape Selective Catalysis in Industrial Applications, Dekker, New York, 1996.
[6] J. Rigoreau, S. Laforge, N.S. Gnep, M. Guisnet, J. Catal. 236 (2005) 45.
[7] S. Laforge, P. Ayrault, D. Manin, M. Guisnet, Appl. Catal. A 279 (2005) 79.
[8] F. Bauer, E. Bilz, A. Freyer, Appl. Catal. A 289 (2005) 2.
[9] F. Bauer, W.H. Chen, H. Ernst, S.J. Huang, A. Freyer, S.B. Liu, Micropor. Mesopor. Mater. 72 (2004) 81.
[10] A. Corma, F. Llopis, J.B. Monton, W. Haag, S. Csicsery, J. Lercher, A. Vannice, V. Fahore, R. Kumar, D. Barthomeuf, A. Tsuganenko, W.C. Conner, Stud. Surf. Sci. Catal. 75 (1993) 1145.
[11] Ch.W. Jones, S.I. Zones, M.E. Davis, Appl. Catal. A 181 (1999) 289.
[12] F. Llopis, G. Sastre, A. Corma, J. Catal. 227 (2004) 227.
[13] D.H. Olson, W.O. Haag, ACS Symp. Ser. 248 (1984) 275.

[14] P. Wagner, S.I. Zones, M.E. Davis, R.C. Medrud, Angew. Chem. Int. Ed. 38 (1999) 1269.
[15] A. Corma, M.J. Diaz-Cabañas, L.J. Martinez-Triguero, F. Rey, J. Rius, Nature 418 (2002) 514.
[16] Y. Mathieu, J.-L. Paillaud, P. Caullet, N. Bats, Micropor. Mesopor. Mater. 75 (2004) 13.
[17] A. Corma, F. Rey, J. Rius, M.J. Sabater, S. Valencia, Nature 431 (2004) 287.
[18] K.G. Strohmaier, D.E.W. Vaughan, J. Am. Chem. Soc. 125 (2003) 16035.
[19] J.-L. Paillaud, B. Harbuzaru, J. Patarin, N. Bats, Science 304 (2004) 990.
[20] A. Burton, S.E. Elomari, R.C. Medrud, I.Y. Chen, C.-Y. Chen, L.M. Bull, E.S. Vittoratos, J. Am. Chem. Soc. 125 (2003) 1633.
[21] M.E. Leonowicz, J.A. Lawton, S.L. Lawton, M.K. Rubin, Science 264 (1994) 1910.
[22] R.F. Lobo, M.E. Davis, J. Am. Chem. Soc. 117 (1995) 3766.
[23] A. Corma, M.T. Navarro, F. Rey, J. Rius, S. Valencia, Angew. Chem. Int. Ed. 40 (2001) 2277.
[24] T. Boix, M. Puche, M.A. Camblor, A. Corma, US Patent 6471941 B1, 2000.
[25] A. Corma, M. Puche, F. Rey, G. Sankar, S.J. Teat, Angew. Chem. Int. Ed. 42 (2003) 1156.
[26] T.R. Forester, W. Smith, J. Mol. Graphics 14 (1996) 136.
[27] M.P. Allen, D. Tildesley, Molecular Simulation of Liquids, Oxford Univ. Press, 1980.
[28] C.R.A. Catlow, C.M. Freeman, B. Vessal, S.M. Tomlinson, M. Leslie, J. Chem. Soc. Faraday Trans. 87 (1991) 1947.
[29] T. Oie, T.M. Maggiora, R.E. Christoffersen, D.J. Duchamp, Int. J. Quantum Chem. Quantum Biol. Symp. 8 (1981) 1.
[30] Ch. Baerlocher, W.M. Meier, D.H. Olson, Atlas of Zeolite Framework Types, fifth ed., Elsevier, 2001. Also in URL, http://www.iza-online.org.
[31] R. Castañeda, A. Corma, V. Fornes, J. Martinez-Triguero, S. Valencia, J. Catal. 238 (2006) 79.
[32] H. van Koningsveld, H. van Bekkum, J.C. Jansen, Acta Crystallogr. B 43 (1987) 127.
[33] A. Corma, E. Benazzi, H. Cauffriez, M.J. Diaz-Cabañas, M.S. Grande-Casas, M.A. Camblor, G. Mabilon, EP 855369.
[34] (a) J.B. Higgins, R.B. LaPierre, J.L. Schlenker, A.C. Rohrman, J.D. Wood, G.T. Kerr, W.J. Rohrbaugh, Zeolites 8 (1988) 446;
(b) J.M. Newsam, M.M.J. Treacy, W.T. Koetsier, C.B. Gruyter, Proc. R. Soc. London A 420 (1988) 375.
[35] C.A. Emeis, J. Catal. 141 (1993) 347.
[36] M. Guisnet, N.S. Gnep, S. Morin, Micropor. Mesopor. Mater. 35–36 (2000) 47.
[37] P. Meriaudeau, V.A. Tuan, V.T. Nghiem, F. Lefebvre, V.T. Ha, J. Catal. 185 (1999) 378.
[38] P. Wu, T. Komatsu, T. Yashima, Micropor. Mesopor. Mater. 22 (1998) 343.
[39] A. Corma, J. Catal. 216 (2003) 406.
[40] J.A. Martens, J. Pérez-Pariente, E. Sastre, A. Corma, P.A. Jacobs, Appl. Catal. 45 (1988) 85.
[41] L.B. Young, S.A. Butter, W.W. Kaeding, J. Catal. 76 (1982) 418.
[42] D.H. Olson, W.O. Haag, ACS Symp. Ser. 248 (1984) 275.
[43] H. Du, D.H. Olson, J. Phys. Chem. B 106 (2002) 395.
[44] T. Amemiya, E. Tsunetomi, E. Nakamura, T. Nakazawa, Bull. Jpn. Petrol. Inst. 3 (1961) 14.
[45] F. Lemos, F.R. Ribeiro, M. Kern, G. Giannetto, M. Guisnet, Appl. Catal. 39 (1988) 227.